Published in final edited form as:
Nanomedicine (Lond). 2010 October ; 5(8): 1183–1191. doi:10.2217/nnm.10.70.

Magnetic resonance lymphangiography with a nano-sized gadolinium-labeled dendrimer in small and large animal models

Laureen M Sena[1], **Steven J Fishman**[1], **Kathy J Jenkins**[1], **Heng Xu**[2], **Martin W Brechbiel**[2], **Celeste AS Regino**[2], **Nobuyuki Kosaka**[2], **Marcelino Bernardo**[2], **Peter L Choyke**[†,2], and **Hisataka Kobayashi**[2]

[1]Boston Children's Hospital, Boston, MA, USA

[2]National Cancer Institute, Bethesda, MD, USA

Abstract

Aim—Imaging of the lymphatic system is critical in preoperative planning of resections of complex lymphatic malformations. However, safe, effective imaging methods with sufficient resolution to identify the lymphatics have been lacking. In this study, we demonstrate the use of gadolinium-labeled dendrimers to image the lymphatics in small and large animal models during magnetic resonance lymphangiography.

Methods—Polyamidoamine G6-Gd_1B4M_*N*-hydroxysuccinimide was synthesized and administered intradermally in the extremities of normal mice and pigs at several doses.

Results—The lymphatics were well demonstrated in both animal models and there was rapid uptake in the deep lymphatic system, including the thoracic duct. A significant dose reduction was achieved (1 μmol Gd/kg) in the 35-kg pig compared with mice, while still producing excellent results. No toxicity was observed and only minor inflammatory changes were observed at the injection site 30 days later.

Conclusion—We demonstrate that a low dose of a macromolecular magnetic resonance contrast agent can provide rapid imaging of the deep lymphatic system in both small and large animals. This data provides a basis to consider a similar agent in clinical trials.

Keywords

dendrimer; magnetic resonance lymphangiography; nanomaterials; pig; thoracic duct

Despite the growing recognition of the role of the lymphatics in health and disease, techniques to visualize the lymphatic channels have lagged behind other imaging methods of the cardiovascular system. This is largely due to the difficulty in accessing the lymphatics, which require either direct cannulation of the small, delicate vessels or interstitial injection [1]. In comparison, the blood vessels can be directly enhanced with a relatively

[†]Author for correspondence: Molecular Imaging Program, National Cancer Institute/National Institutes for Health, Building 10, Room B3B69, Bethesda, MD 20892-1088, USA, Tel.: +1 301 402 8409, Fax: +1 301 402 3191, pchoyke@nih.gov.

Financial & competing interests disclosure
The authors have no other relevant affiliations or financial involvement with any organization or entity with a financial interest in or financial conflict with the subject matter or materials discussed in the manuscript apart from those disclosed.
No writing assistance was utilized in the production of this manuscript.

Ethical conduct of research
The authors state that they have obtained appropriate institutional review board approval or have followed the principles outlined in the Declaration of Helsinki for all human or animal experimental investigations. In addition, for investigations involving human subjects, informed consent has been obtained from the participants involved.

straightforward intravascular injection. Existing lymphatic imaging techniques include lymphoscintigraphy, in which a ^{99m}Tc-labeled sulfur colloid or similar macromolecule is injected interstitially and serial imaging is performed [2]. This technique has been useful in sentinel node detection and in lymphedema studies, but its low spatial resolution prevents it from being used to visualize individual lymphatic channels. Direct x-ray lymphangiography, which employs an intra-lymphatic injection of an oily iodinated contrast agent (e.g., lipiodol) followed by serial radiographs, has been largely abandoned due to its invasiveness [2]. MRI, which has proven so valuable in imaging other organs, has had a relatively minor role in the imaging of the lymphatics [2–4].

There are compelling clinical reasons to develop an imaging agent for the lymphatics. In addition to visualizing sentinel nodes for cancer staging [5], there is a clinical need to map the lymphatic vasculature of lymphatic malformations/anomalies and traumatic lymphatic interruptions prior to resection [6–11]. The understanding and treatment of human tumors, which induce and spread by lymphangiogenesis, would also benefit from methods that permit visualization and quantitation of individual lymphatic structures [12–14].

Identifying the lymphatic channels themselves requires a modality with high spatial resolution and high sensitivity for contrast agents, since the lymphatic channels themselves are so small. The lymphatic circulation is passively driven by a combination of negative pressure in the thorax and positive pressure from muscles surrounding the lymphatics. Local pressure (e.g., swelling or edema) also drives the lymphatic circulation. Therefore, the thermophysical movement of molecules strongly affects the efficacy of drainage from the interstitium. Even so, experience has shown that the lymphatics are highly selective for nano-sized molecules. Smaller molecules (<6 nm) are poorly absorbed by the lymphatics and disperse by convection [15,16]. Larger molecules (>20 nm) are eventually taken up by the lymphatics, but this occurs slowly and the rate is dependent on molecular size. In addition, from the biological safety point of view, since the lymphatics eventually connect to the vascular circulation, it is preferable that the contrast agent be excreted through the kidney [17,18]. Thus, the characteristics of an optimal lymphatic imaging agent is one that is both taken up and retained by the lymphatics, whilst providing adequate concentration for imaging, and which is then excreted in the urine.

In this article, we present the first experience, in both small and large animal models, demonstrating that a dendrimer-based gadolinium (Gd)-labeled contrast agent can successfully visualize the deep lymphatic system within minutes of its interstitial injection. The agent was tolerated well with minimal adverse events and is a candidate for clinical translation.

Materials & methods

Synthesis of G6-Gd_1B4M_NHS

The synthesis of the *tert*-butyl form of the 1B4M_*N*-hydroxysuccinimide (NHS) has been previously reported [19]. This NHS ester chelate is an amine reactive form that can enable the conjugation of the chelate to the terminal amino groups of the generation (G)-6 polyamidoamine dendrimer via the formation of a stable amide bond.

Conjugation of the bifunctional chelate to the dendrimer and subsequent deprotection and Gd complexation was performed following previously described methods using the G6 dendrimer instead of G4 dendrimer (Aldrich Inc., MO, USA) [19]. The product was then dialyzed exhaustively with water using a tangential flow filtration system (Millipore, Billerica, MA, USA) equipped with a Pellicon XL 50 cm^2 BIOMAX 10 cassette (Millipore,

Billerica, MA, USA). The residual solution was then sterile-filtered through a 0.22-μm filter into a sterile flask and lyophilized to obtain a white solid.

Supplementary Figure 1 (see online www.future-medicine.com/doi/suppl/10.2217/nnm.10.70) summarizes the synthesis of the *N*-hydroxysuccinimidyl ester of the *tert*-butyl protected form of the chelate.

Figure 1 summarizes the conjugation of the 1B4M_NHS chelate to G6 polyamidoamine dendrimer and Gd(III) complexation to G6–1B4M_NHS.

Characterization of G6-Gd_1B4M_NHS

Purity was assessed using size-exclusion highperformance liquid chromatography (SE-HPLC) shown in Supplementary Figure 2 on a TSK-GEL® G2000SW column with a retention time of 11.3 min and on a TSK-Gel G6000PW column with a retention time of 20.5 min (estimated hydrodynamic size based on protein standards ~13 nm) (Figure 2, Supplementary Figure 2).

Elemental analyses were performed by Columbia Analytical Services, Inc. (formerly Desert Analytics; Tucson, AZ, USA) using a combustion analysis method for C, H and N, and inductively coupled plasma-atomic emission spectroscopy for determining the percentage of Gd. Samples were analyzed in duplicates. Analysis was calculated for $[G6(Gd1B4MNHS)_{155}(1B4M\_\ NHS)_{35}(C_6H_7O_7)_{50}Na_{200}(H_2O)_{675}]$ (C: 42.66; H: 5.48; N: 11.11; Gd: 10.87). As shown in the synthesis method reported previously [17], sodium gluconate buffer was used for chelating Gd ions. Therefore, although the sample for this elemental analysis was dialyzed against the metal-free distilled water, sodium, keto-gluconate and water remained in the lyophilized sample.

The hydrodynamic radius of the G6-Gd_1B4M_ NHS was assessed using dynamic light scattering measurements, which approximated the size at 17 nm in 1 × phosphate-buffered saline (PBS).

Magnetic resonance contrast enhancement properties (r_1 and r_2) were determined from dilute solutions of the contrast agent G6-Gd_1B4M_NHS. Brief ly, solutions of G6-Gd1B4M (0.25–1.0 mM) in 1 × PBS (300 μl) were prepared along with a corresponding set from Gd-diethylene-triamine-pentaacetic acid (DTPA; Magnevist, Bayer HealthCare Pharmaceuticals, Montville, NJ, USA) used as standards. Images were obtained at approximately 22°C using a 3-tesla clinical scanner (Signa Excite, General Electric Medical System, Waukesha, WI, USA) equipped with a rectangular surface single loop coil (84 × 126 × 6 mm). Images of the solutions using a 2D-spin echo sequence were acquired for T1 calculation with repetition times (TR) of 167, 300, 617, 1250, 2500 and 5000 ms all at an echo time (TE) of approximately 9 ms, an 8-echo 2D-spin echo sequence with a TR of 5000 ms and a TE interval of approximately 8.5 ms for T_2 calculation. T_1 and T_2 maps were created using ImageJ MRI Analysis plug-in [101]. T_1 and T_2 relaxivities, r_1 and r_2, were determined from the slopes of the plot of relaxation rates, $r_1 = 1/T_1$ and $r_2 = 1/T_2$, versus [Gd] (Table 1).

Serum stability studies of G6-Gd_1B4M_NHS

^{153}Gd was incorporated into the final product; G6-Gd_1B4M_NHS was created by the addition of 600 μCi of ^{153}Gd to a solution of G6-Gd_1B4M_NHS (500 μg) in 0.15 M NH_4OAc at pH 4.5. This radioactively spiked solution was allowed to react for 1 h at room temperature before being quenched with 10 μl of 0.1 M EDTA. The G6-[^{153}Gd]Gd_1B4M_NHS was then purified by exhaustive dialysis using an Amicon Ultra-15 (MWCO 30,000)

centrifugal filter device (Millipore, Billerica, MA, USA) against 1 × PBS. Approximately 471 μCi of the G6-[^{153}Gd]Gd_1B4M_NHS was obtained from this reaction.

Approximately 400 μCi of G6-[^{153}Gd]-Gd_1B4M_NHS in 150 μl of 1 × PBS was added to 600 μl of human serum (Gemini Bio Products, West Sacramento, CA, USA) to bring the total volume to 750 μl. Thereafter, a 150 μl aliquot of this solution was placed in 5–1 ml microtubes. These serum samples were incubated at 37°C and 350 rpm. At each time point after incubation with human serum (0, 1, 2, 3, 4, 5, 6 and 7 days, and then once every week up to 6 weeks), 5 μl of 0.1 M EDTA was added to a 5-μl aliquot serum sample to attach the released Gd ions to the serum protein, and the sample was analyzed by radio SE-HPLC using a Superose™ 12 10/300 column (GE Life Sciences, Piscataway, NJ, USA) eluted with 1 × PBS at 0.5 ml/min for 1 h. The release of ^{153}Gd radionuclide from the G6-[^{153}Gd] Gd_1B4M_NHS was monitored with the released ^{153}Gd (if any) captured by EDTA being eluted at approximately 40 min, while the product eluted at approximately 21 min (Figure 3).

In vivo magnetic resonance lymphangiography studies *In vivo* studies in mice

A total of f ive 8-week-old normal athymic (nu/nu) female mice (Charles River Laboratories, Wilmington, MA, USA) were used to evaluate the G6-Gd_1B4M_NHS's ability to visualize the lymphatics. All procedures were performed in accordance with the NIH guidelines on the use of animals in research and were approved by the Animal Care and Use Committee of the National Cancer Institute. The mice were chemically restrained using 2% isoflurane (IsoFlo, Abbott Laboratories, Abbott Park, IL, USA) in O_2 delivered using a Summit Anesthesia Solution vaporizer (Bend, OR, USA) at a flow rate of approximately 1.0 ml/min. Intracutaneous injections of 10 μl each of 30 mM in Gd (300 μM) of the G6-Gd_1B4M_ NHS were administered in the middle phalanges of both upper extremities, similar to the previously reported procedure [4,20]. Dynamic magnetic resonance (MR) images were obtained immediately after injections (<2 min) by repeating the 3D fast spoiled gradient recalled echo (3D-fSPGR) with chemical fat suppression (Signa Excite 3-tesla, TR/TE of ~11/4 ms at 30° flip angle) approximately every 5 min for 30 min to monitor the lymphatic drainages in the axillary and lateral thoracic lymph nodes. Images were processed using ImageJ [102] and maximum intensity projections were calculated from the resulting 3D images.

In vivo studies in large animals

In the study, 3-month-old pigs (n = 7) that were 30–35 kg were used for testing. All procedures were performed in accordance with the Boston Children's Hospital guidelines on the use of animals in research and were approved by the Animal Care and Use Committee (protocol number A06–07–050). After an overnight fast, the animal was preanesthetized with atropine 0.04 mg/kg, Terazol 4.4 mg/kg and xylazine 2 mg/kg intramuscularly. The animal was transferred to the MRI scanner (1.5T Achieva, Philips Healthcare, Cleveland, OH, USA) on a water circulation heating pad. An intravenous line was placed using aseptic technique into the auricular marginal vein and intravenous fluids (lactated ringers or 0.9% saline) were administrated. Electrocardiography pads and electrodes were placed over the shaven metacarpal and metatarsal areas as well as the chest wall for vital sign monitoring and MRI gating. For the duration of the study, the adequacy of anesthesia was continuously assessed using clinical parameters (e.g., heart rate, respiratory rate and level of sedation), hemodynamic measurement (systemic arterial pressure) and noninvasive oxygen saturation.

When the animal reached an adequate anesthetic plane (gas mask with 1–2% isoflurane) it was intubated with an appropriate size endotracheal tube. The cuff on the endotracheal tube was inflated to prevent leakage and assure adequate ventilation, and it was tied into place to

prevent dislodgement during the procedure. The animal was then placed on the table and connected to the anesthetic machine and ventilator. General anesthesia was maintained with inhaled 1–2% isoflurane delivered through a precision vaporizer and a circle absorption breathing system.

After achieving an adequate and hemo-dynamically stable anesthesia, the animal was transported into the MRI room. Once in the scanner room, the animal was connected to the MRI compatible anesthetic machine and ventilator (Surgivet, Smiths Medical PM, Inc., Waukesha, WI, USA). General anesthesia was maintained with inhaled isoflurane (1–2%) through a precision vaporizer and a circle absorption breathing system. For the duration of the study, the animal's vital signs (e.g., heart rate, respiratory rate, O_2 pulse oximetry and end-tidal CO_2) were acquired every 15 min with an MRI compatible physiological monitoring system (*In vivo* Systems, Orland, FL, USA).

G6-Gd_1B4M_NHS was administered by intradermal injection into a hind foot in seven pigs. MRI was performed with a phased array surface coil using a 3D thoracic T1-weighted sequence with fat saturation (TR: 5 ms; TE: 2.4 ms; slice thickness: 1.5 mm [×95 slices]; five averages; flip angle: 10°; FOV: 38 cm; echo train length: 50; acquisition matrix: 368 × 371; reconstruction matrix: 528 × 528; acquisition time: 201 s) in the coronal plane for 15 min (3–4 min imaging time), then at 15-min intervals for 1–2 h. Since the pig was positioned on its side, coronal imaging effectively produced images in the sagittal plane. Histology was performed on the hoof 30 days postinjection in two animals.

Results

Quality control & serum stability

A bifunctional DTPA derivative, 1B4M-DTPA, was used to conjugate the chelate to the dendrimer construct for Gd complexation. The chelate, 1B4M-DTPA, has been established to form stable metal complexes *in vivo* and *in vitro* [17]. The amide linkage, formed from the reaction of the NHS activated bifunctional chelate and the terminal amine of the dendrimer construct, utilized in the conjugation of the bifunctional chelate to the G6 dendrimer, possessed well-established stability and usage. Excess bifunctional chelate (~1.5-fold) and excess Gd(III) (~1.5-fold) per terminal amino group was used to maximize the number of chelates and Gd(III)–chelate complex, respectively, on the surface of the dendrimer construct. Removal of the nonconjugated bifunctional chelate and uncomplexed Gd(III) was achieved through exhaustive diafiltration and monitored by SE-HPLC.

The average number of chelates covalently conjugated to the surface of polyamidoamine ethylendiamine dendrimer was estimated from elemental analysis to be approximately 190 (74% saturation) out of the 256 theoretically available terminal amino groups in the G6 dendrimer. This saturation yield is attributed to the decreasingly available terminal groups with increasing steric hindrance encountered as the conjugation reaction proceeds, and also due to the presence of imperfections in the core dendrimer that results in less than the ideal 256 terminal amino groups. The average number of Gd(III) incorporated in the chelate–dendrimer construct, G6 1B4M_ NHS, was established through a combination of inductively coupled plasma mass spectrometry and elemental analysis, and determined to be approximately 155 (82% of the available chelate) per chelate–dendrimer construct.

The r_1 and r_2 relaxivities at 3T of the G6-Gd_1B4M_NHS were 10.75 ± 0.48 and 30.24 ± 0.02 $mM^{-1}s^{-1}$, respectively, versus 4.45 ± 0.02 and 5.47 ± 0.07 $mM^{-1}s^{-1}$, respectively, for Gd-DTPA (Magnevist). The increase in the relaxivities (r_1 and r_2) of the G6-Gd_1B4M_NHS was observed to correlate with the increased molecular size of the Gd(III) dendrimer-based MR agents [21,22].

The stability of G6-Gd_1B4M_NHS *in vitro* using human serum was assessed by measuring the release of ^{153}Gd radionuclide from the G6-Gd_1B4M_NHS construct. The G6-Gd_1B4M_NHS demonstrated serum stability up to 6 weeks, the latest time point in the study, and showed no release of Gd ion into the serum.

In vivo studies in mice

Major lymph nodes (axillary and lateral thoracic lymph nodes) that drain the upper extremities were clearly visualized immediately after injection by 3D micromagnetic resonance lymphangiography using the G6-Gd_1B4M (Figure 4) in all mice. In addition, the deep lateral thoracic lymph node and the thoracic duct connecting it to the axillary lymph node were also visualized. This is consistent with previous studies of similar macromolecular dendrimer-based Gd contrast agent [20].

In vivo studies in pigs

Seven pigs underwent MR lymphangiography with hind foot injections followed by serial thoracic MRI. In this dose-ranging study, the first pig received approximately 3 ml of 120 mM Gd (Gd dose= 12 μmol Gd/kg). This injected amount resulted in excessive amounts of contrast in the thoracic duct, which cleared slowly. Therefore, the next dose was reduced to 25% of the initial dose, 3 ml of 30 mM Gd (Gd dose = 3 μmol Gd/kg), which produced opacification of the thoracic duct within 5 min. The dose was reduced further by using only 1 ml of 30 mM Gd (Gd dose = 1 μmol Gd/kg) and although the thoracic duct was visualized it was not as intense and took 15 min to visualize. This result determined that the 3 ml injection volume was important in creating sufficient interstitial pressures to rapidly image the thoracic duct. The next dose reduction was to lower the concentration of the injectate and use 3 ml of 10 mM Gd (Gd dose 1 μmol Gd/kg). This produced rapid (within 5 min) opacification of the thoracic duct. An attempt to further reduce the dose (3 ml of 3.3 mM Gd; Gd dose = 0.3 μmol Gd/kg) produced relatively weak opacification of the thoracic duct, which defined this concentration as too low. Therefore, we established a dose of 3 ml of 10 mM Gd (Gd dose = 1 μmol Gd/kg) as optimal and completed two more animals at this dose, both with similar results. It should be noted that the standard clinical dose of intravenous Gd chelates is typically 0.1 mmol Gd/kg or 100 μmol Gd/kg. Thus, the dose proposed for MR lymphangiography is approximately 1/100th the clinical intravascular dose (Figure 5).

No immediate effects were observed in respiratory rate, heart rate or percentage hemoglobin saturation. Mild inflammatory changes were seen in the skin at the site of the injection compared with the contra lateral skin, where PBS was injected.

Discussion

Previous experiments have shown that the optimal size for a lymphatic imaging agent lies in the range of 6 to 20 nm [15–18]. While there are several options for nanoparticles in this range, such as albumin and immunoglobulins, these generally do not permit the conjugation of a sufficient number of Gd chelates to permit imaging with a small volume of injectate. Dendrimers are polymers that branch geometrically from a central core. Terminal amine groups permit the conjugation of multiple Gd chelates. Thus, we have selected the G6-Gd_1B4M_NHS (with approximately 150–200 Gd/dendrimer) as a favorable lymphatic imaging agent with an excellent T_1 relaxivity. In addition, G6-Gd_1B4M_NHS dendrimer has the advantage of threefold higher relaxivity than existing US FDA-approved Gd-chelates at 3-tesla and even higher relaxivities at 1.5-tesla [20].

The scale-up of the synthesis for large animal imaging requires a new conjugation method using an organic solvent, similar to previously published methods [19]. The G6-

Gd_1B4M_NHS was tested in mice (weight ~20 g) at a dose of 0.015 mmol Gd/kg (30 mM Gd/10 μl per mouse) and showed excellent delineation of the lymphatics within minutes of injection. As demonstrated in this study, this agent was successful in pigs weighing approximately 30 kg or 1000- times the weight of a mouse. Surprisingly, the dose required was even lower than that required for mice (1 μmol Gd/kg, 10 mM Gd/3 ml in 30-kg pigs). Since the lymphatic circulation, which is a one-way circulation, does not recirculate, the volume of the lymphatic system per unit body weight might be larger in rodents than in the large animals. This Gd dose is approximately 1% of the US FDAapproved dose for intravenous application of Gd chelates. Furthermore, the dendrimer dose is only approximately 5 nmol/kg, which is generally considered in the range of a 'microdose' from a regulatory standpoint. Lower concentrations (0.0003 mmol Gd/kg) unfortunately resulted in compromised images. When the injection volume was reduced from 3 to 1 ml, visualization of the lymphatics was slowed and reduced in intensity, indicating that the volume of injection and its attendant increase in interstitial pressure at the injection site is important for rapid uptake by the lymphatics. Thus, excellent visualization of the deep lymphatic system was achieved with a very modest dose and volume of the G6-Gd_1B4M_NHS in a large (30 kg) animal model.

All animals tolerated the injection well. The animals were monitored for respiratory rate and heart rate. No changes related to the injection were observed. This is in keeping with the low dose of injection. Histology performed on the injected limbs at 30 days revealed only mild inflammatory changes at the injection site, commensurate with an interstitial injection. The agent was filtered and therefore unlikely to contain bacteria, but was not tested for endotoxins, and this may be the source of the inflammation.

Limitations of this study include the small number of animals scanned. However, the results were very consistent among the animals that were injected at the optimal dose. In addition, although there was no evidence of nephrogenic sclerosing fibrosis, the chelate used (1B4M-DTPA) had a lower stability constant (K_d) than some macrocyclic chelates (e.g., 1,4,7,10-tetraazacyclododecane-1,4,7,10-tetraacetic acid [DOTA]). Given the intense scrutiny that current Gd chelates are receiving by regulatory agencies, such as the FDA, alternative chelates are being considered for clinical versions. Only immediate and 30-day side effects were evaluated in this study, so more comprehensive toxicity testing will be needed before clinical trials in humans commence.

Conclusion

We have demonstrated that G6-Gd_1B4M_NHS injected interstitially is rapidly taken up by the deep lymphatic system in both small and large animal models. The Gd dose required for large animals is approximately 1% of the intravenous Gd dose of small Gd chelates for conventional MR studies. This opens up the possibility of imaging the lymphatic system for preoperative lymphatic mapping for surgical planning and the study of lymphangiogenesis in humans.

Future perspective

Gadolinium-conjugated dendrimers hold great promise as imaging agents for the lymphatic system. We have shown that such a conjugate, despite being administered at a very low dose in large animals, retains the ability to depict the lymphatic channels with MRI. This opens up the possibility of developing a similar agent for human use in order to evaluate lymph edema, lymphatic malformations in children and sentinel nodes in patients with cancer.

Supplementary Material

Refer to Web version on PubMed Central for supplementary material.

Acknowledgments

This research was supported in part by the Intramural Research Program of the NIH, National Cancer Institute, Center for Cancer Research.

Bibliography

Papers of special note have been highlighted as:

■ of interest

■■ of considerable interest

1. Sharma R, Wendt JA, Rasmussen JC, Adams KE, Marshall MV, Sevick-Muraca EM. New horizons for imaging lymphatic function. Ann. NY Acad. Sci. 2008; 1131:13–36. [PubMed: 18519956]
2. Barrett T, Choyke PL, Kobayashi H. Imaging of the lymphatic system: new horizons. Contrast Media Mol. Imaging. 2006; 1(6):230–245. [PubMed: 17191764] ■ Excellent review article on the basis and application of lymphatic imaging.
3. Kobayashi H, Kawamoto S, Sakai Y, et al. Lymphatic drainage imaging of breast cancer in mice by micro-magnetic resonance lymphangiography using a nano-size paramagnetic contrast agent. J. Natl Cancer Inst. 2004; 96(9):703–708. [PubMed: 15126607]
4. Kobayashi H, Kawamoto S, Star RA, Waldmann TA, Tagaya Y, Brechbiel MW. Micro-magnetic resonance lymphangiography in mice using a novel dendrimer-based magnetic resonance imaging contrast agent. Cancer Res. 2003; 63(2):271–276. [PubMed: 12543772] ■ First paper describing lymphatic MRI using a dendrimer-based contrast agent.
5. Benson JR, Jatoi I, Keisch M, Esteva FJ, Makris A, Jordan VC. Early breast cancer. Lancet. 2009; 373(9673):1463–1479. [PubMed: 19394537]
6. Nair SK, Petko M, Hayward MP. Aetiology and management of chylothorax in adults. Eur. J. Cardiothorac. Surg. 2007; 32(2):362–369. [PubMed: 17580118]
7. Cha EM, Sirijintakarn P. Anatomic variation of the thoracic duct and visualization of mediastinal lymph nodes: a lymphographic study. Radiology. 1976; 119(1):45–48. [PubMed: 1257453]
8. McGrath EE, Blades Z, Anderson PB. Chylothorax: aetiology, diagnosis and therapeutic options. Respir. Med. 2010; 104(1):1–8. [PubMed: 19766473]
9. Alomari AI, Karian VE, Lord DJ, Padua HM, Burrows PE. Percutaneous sclerotherapy for lymphatic malformations: a retrospective analysis of patient-evaluated improvement. J. Vasc. Interv. Radiol. 2006; 17(10):1639–1648. [PubMed: 17057006]
10. Burrows PE, Mitri RK, Alomari A, et al. Percutaneous sclerotherapy of lymphatic malformations with doxycycline. Lymphat. Res. Biol. 2008; 6(3–4):209–216. [PubMed: 19093794]
11. Mine S, Udagawa H, Kinoshita Y, Makuuchi R. Post-esophagectomy chylous leakage from a duplicated left-sided thoracic duct ligated successfully with left-sided video-assisted thoracoscopic surgery. Interact. Cardiovasc. Thorac Surg. 2008; 7(6):1186–1188. [PubMed: 18782784]
12. Hoshida T, Isaka N, Hagendoorn J, et al. Imaging steps of lymphatic metastasis reveals that vascular endothelial growth factor-c increases metastasis by increasing delivery of cancer cells to lymph nodes: therapeutic implications. Cancer Res. 2006; 66(16):8065–8075. [PubMed: 16912183]
13. Kakinuma T, Nadiminti H, Lonsdorf AS, et al. Small numbers of residual tumor cells at the site of primary inoculation are critical for anti-tumor immunity following challenge at a secondary location. Cancer Immunol. Immunother. 2007; 56(7):1119–1131. [PubMed: 17139493] ■■ Describes the efficacy of lymphatic MRI for detecting lymphadema.

14. McElroy M, Hayashi K, Garmy-Susini B, et al. Fluorescent LYVE-1 antibody to image dynamically lymphatic trafficking of cancer cells *in vivo*. J. Surg. Res. 2009; 151(1):68–73. [PubMed: 18599080]
15. Kobayashi H, Kawamoto S, Bernardo M, Brechbiel MW, Knopp MV, Choyke PL. Delivery of gadolinium-labeled nanoparticles to the sentinel lymph node: comparison of the sentinel node visualization and estimations of intra-nodal gadolinium concentration by the magnetic resonance imaging. J. Control. Release. 2006; 111(3):343–351. [PubMed: 16490277]
16. Kobayashi H, Kawamoto S, Choyke PL, et al. Comparison of dendrimer-based macromolecular contrast agents for dynamic micro-magnetic resonance lymphangiography. Magn. Reson. Med. 2003; 50(4):758–766. [PubMed: 14523962]
17. Kobayashi H, Brechbiel MW. Nano-sized MRI contrast agents with dendrimer cores. Adv. Drug Deliv. Rev. 2005; 57(15):2271–2286. [PubMed: 16290152] ■ Excellent review describing synthesis, application and experimental details for MRI contrast agents based on gadolinium-dendrimers.
18. Longmire M, Choyke PL, Kobayashi H. Clearance properties of nano-sized particles and molecules as imaging agents: considerations and caveats. Nanomedicine. 2008; 3(5):703–717. [PubMed: 18817471]
19. Xu H, Regino CA, Bernardo M, et al. Toward improved syntheses of dendrimer-based magnetic resonance imaging contrast agents: new bifunctional diethylenetriaminepentaacetic acid ligands and nonaqueous conjugation chemistry. J. Med. Chem. 2007; 50(14):3185–3193. [PubMed: 17552504] ■■ Describes a new chemical conjugation method, which was used in this study.
20. Hama Y, Bernardo M, Regino CA, et al. MR lymphangiography using dendrimer-based contrast agents: a comparison at 1.5t and 3.0t. Magn. Reson. Med. 2007; 57(2):431–436. [PubMed: 17260373]
21. Wiener EC, Brechbiel MW, Brothers H, et al. Dendrimer-based metal chelates: a new class of magnetic resonance imaging contrast agents. Magn. Reson. Med. 1994; 31(1):1–8. [PubMed: 8121264] ■■ First paper to describe a dendrimer-based MRI contrast agent.
22. Konda SD, Aref M, Wang S, Brechbiel M, Wiener EC. Specific targeting of folate-dendrimer MRI contrast agents to the high affinity folate receptor expressed in ovarian tumor xenografts. Magma. 2001; 12(2–3):104–113. [PubMed: 11390265]

Websites

101. MRI Analysis Calculator. www.rsb.info.nih.gov/ij/plugins/mri-analysis.html
102. ImageJ. http://rsb.info.nih.gov/ij/

Executive summary

- We have demonstrated that gadolinium (Gd)-labeled dendrimer-based contrast agents can visualize the deep lymphatics, including the thoracic duct, in both mice and pigs.
- The dose required to visualize the lymphatics in mice (0.015 mmol Gd/kg), while lower than intravenous doses, was significantly greater than the dose needed to visualize the lymphatics in pigs (0.001 mmol Gd/kg).
- The dose in pigs is approximately 1% of the intravenous dose of Gd for current US FDA-approved Gd–chelates (0.1 mmol Gd/kg).
- The results were consistent across animals.
- Histological analysis showed only inflammatory changes at the injection site, most probably due to the mechanical injection pressure.

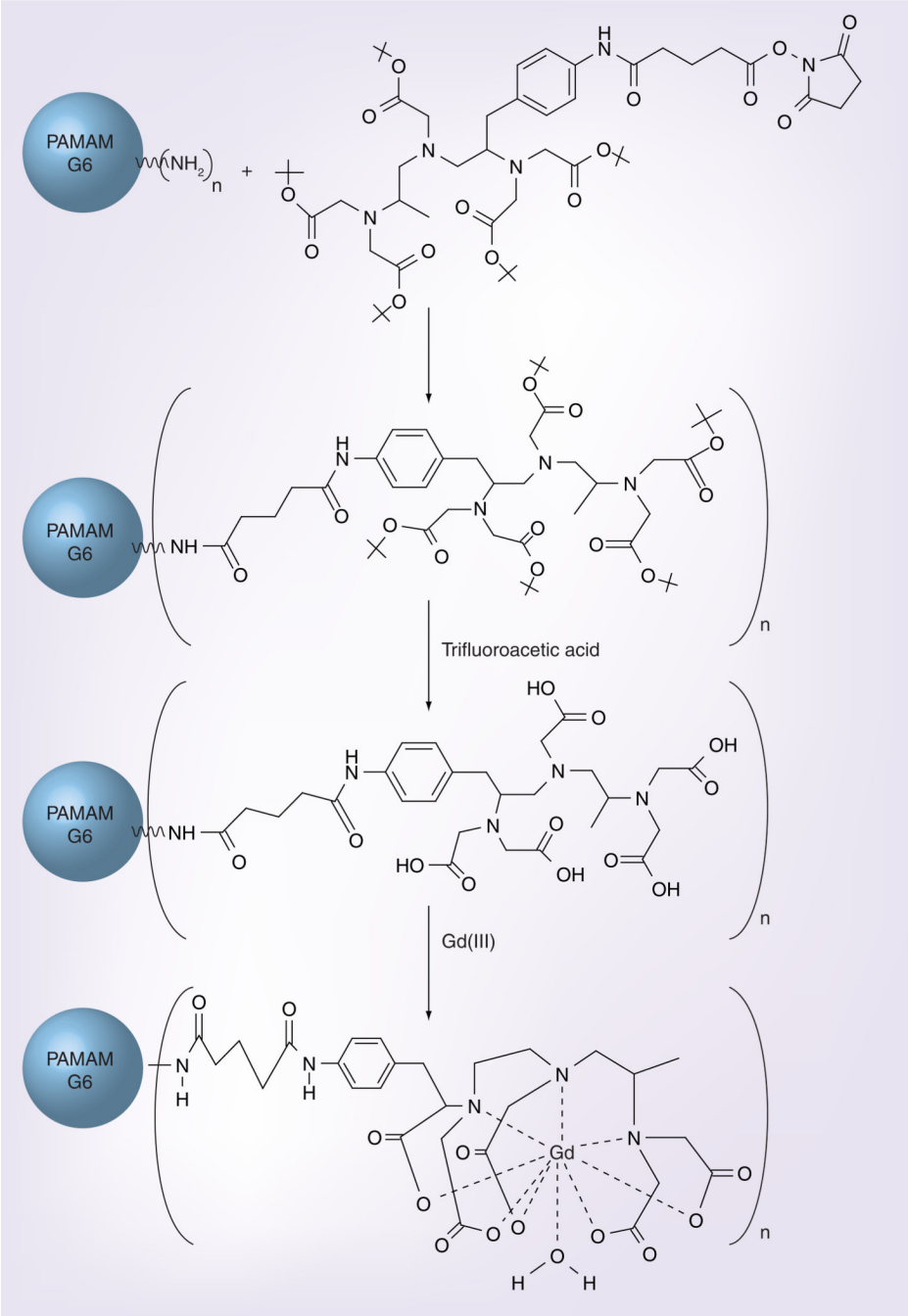

Figure 1. Conjugation of the chelate 1B4M_NHS to generation 6 polyamidoamine dendrimer and incorporation of gadolinium (III) ions to the chelate

Gd: Gadolinium; NHS: *N*-hydroxysuccinimide; PAMAM: Polyamidoamine.

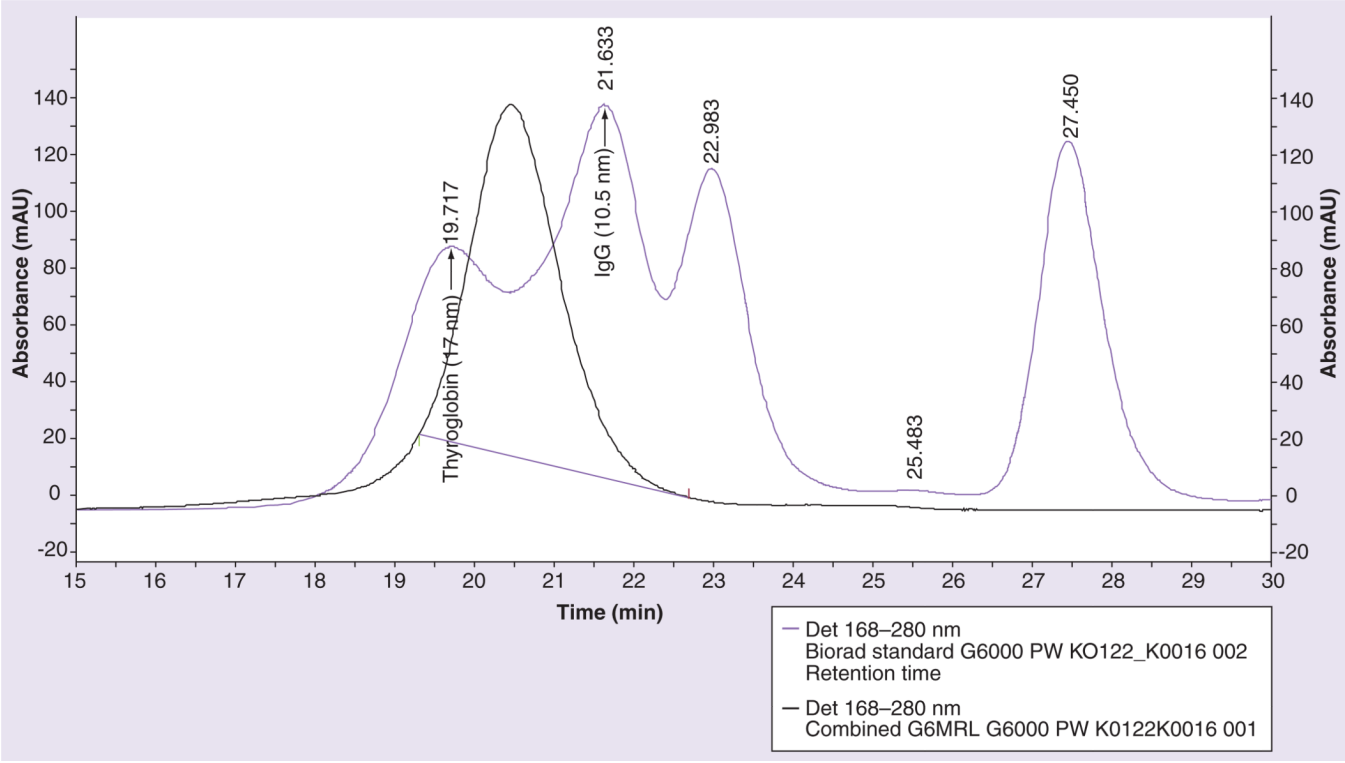

Figure 2. Size exclusion-high performance liquid chromatography chromatogram of the contrast agent G6-Gd_1B4M_NHS (black) and of the Biorad standard protein mixture (purple) on a TSK-Gel G6000PW

The hydrodynamic size of G6-Gd_1B4M is estimated to be approximately 13 nm, in between the thyroglobulin approximately 17 nm, and IgG approximately 11 nm.
Gd: Gadolinium; NHS: *N*-hydroxysuccinimide.

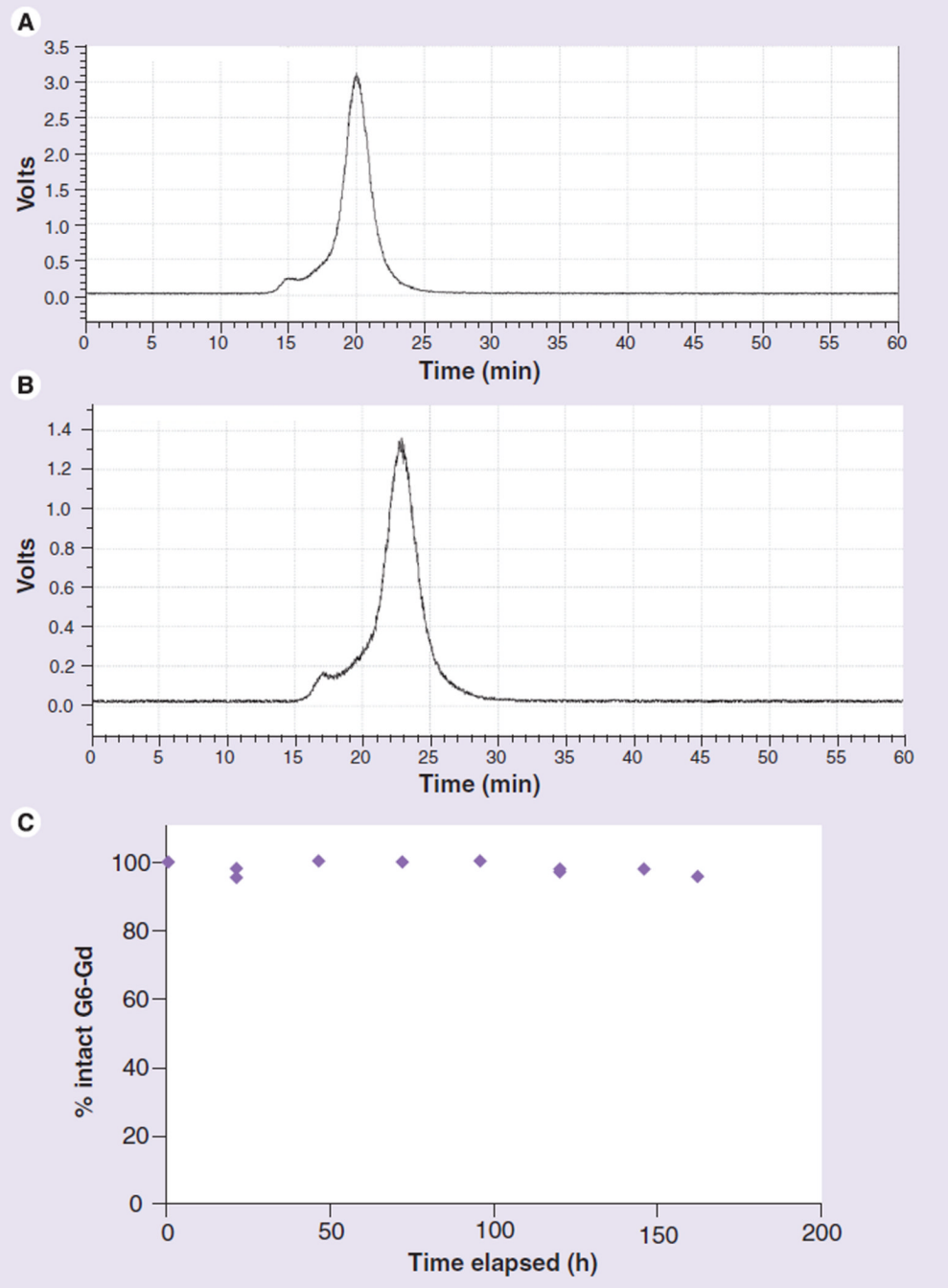

Figure 3. Radio traces of ^{153}Gd-labeled G6-Gd_1B4M_NHS on a Superose™ 12 column eluted at 0.5 ml/min

(A) ^{153}Gd-labeled G6-Gd_1B4M_NHS before addition to the human serum. **(B)** After addition of the ^{153}Gd-labeled product to the human serum. **(C)** Shows the integration of the intact ^{153}Gd-labeled G6-Gd_1B4M_NHS versus any ^{153}Gd being released during the incubation at 37°C.

G: Generation; Gd: Gadolinium; NHS: *N*-hydroxysuccinimide.

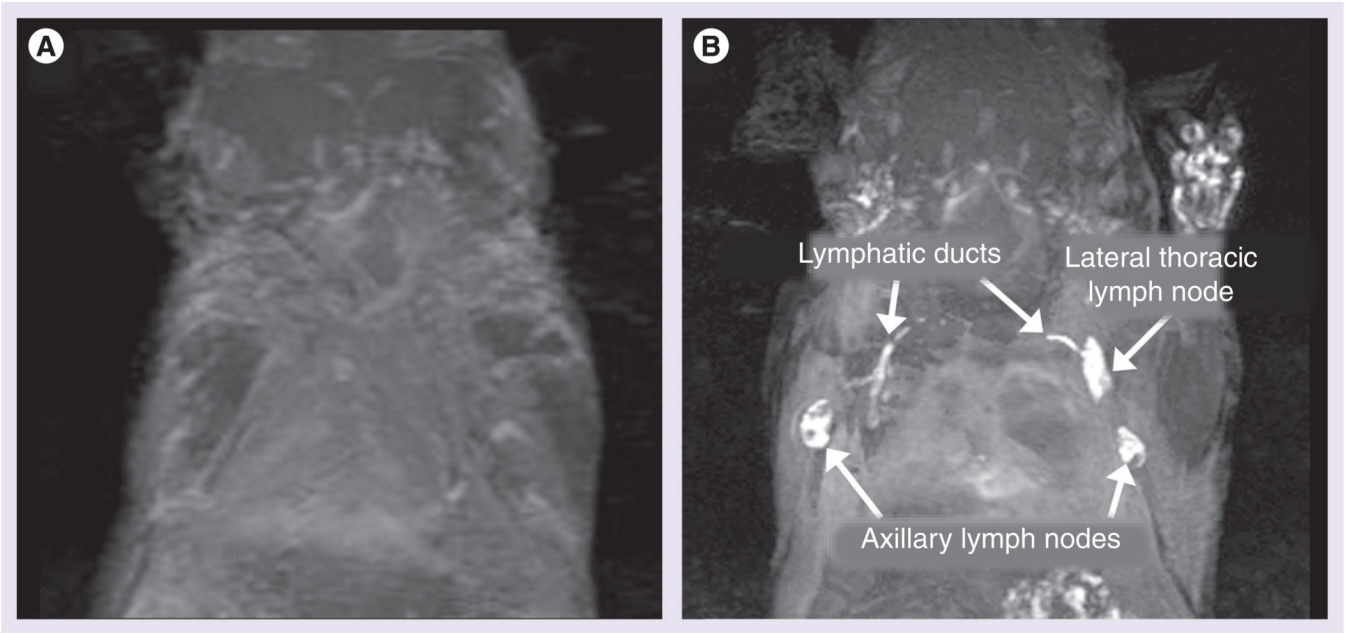

Figure 4. Maximum intensity projection, (A) noncontrast and (B) postcontrast, demonstrating the efficacy of G6-Gd_1B4M_NHS after an intracutaneous injection of the 5 μmol Gd/kg agent on the front paws of an athymic mouse

Lymphatic ducts to the lateral thoracic and axillary lymph nodes are also visualized.
Gd: Gadolinium; NHS: *N*-hydroxysuccinimide.

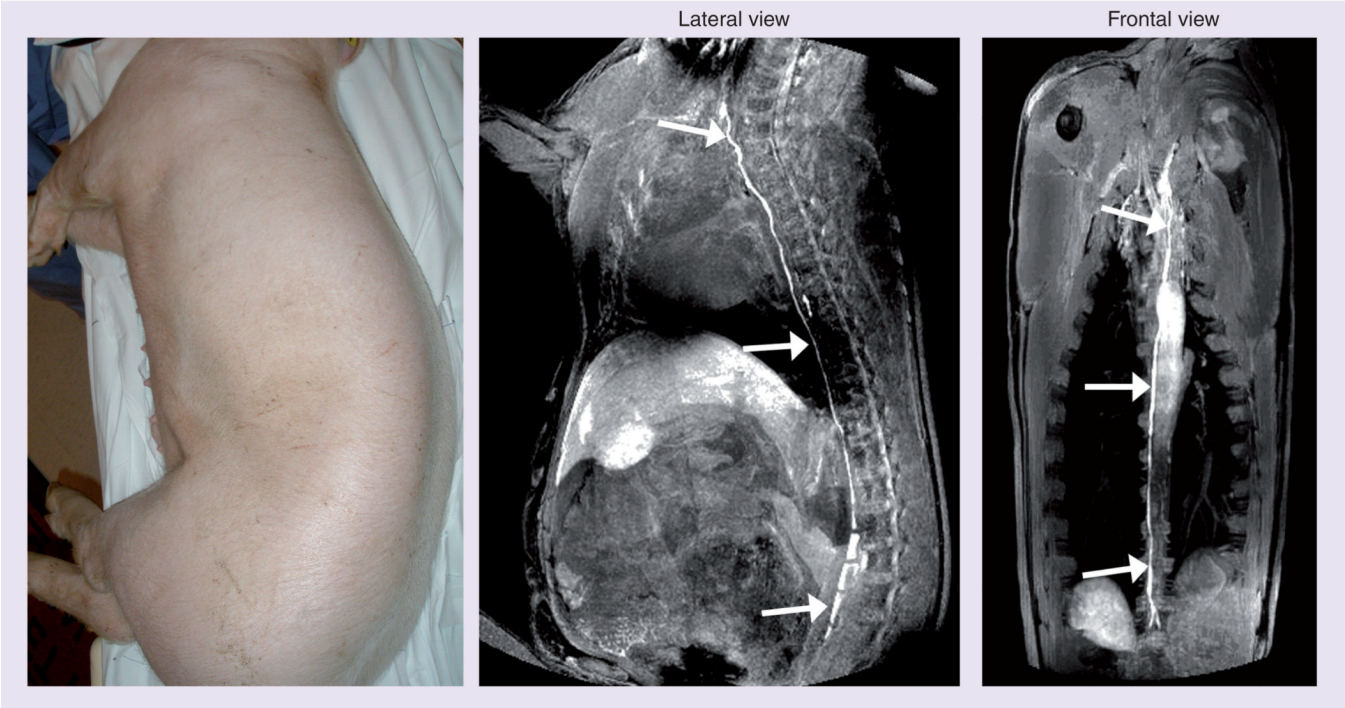

Figure 5. Visualization of the thoracic duct in a 35-kg pig 10 min after injection of 1 μmol Gd/kg (3 ml/10 mM) into the hind limb

Also see Supplementary videos 1 & 2.

Table 1

Properties of G6-Gd_1B4M_NHS.

G6-Gd_1B4M_NHS	Average
Size by DLS, nm (in 1 × PBS)	17
Size by SE-HPLC, nm	13
% Gd by weight	10.85
r_1, /mM/s	10.75
r_2, /mM/s	30.24

DLS: Dynamic light scattering; Gd: Gadolinium; NHS: N-hydroxysuccinimide; PBS: Phosphatebuffered saline; SE-HPLC: Size exclusion-high performance liquid chromatography.